geoconvention
Calgary • Canada • May 15-19 2017

How Do Seismic Event Sizes Scale in the Microseismic Range?

Megan Zecevic[1], Sarah Grant[1], David W. Eaton[1] and Joern Davidsen[2]
[1]Dept. of Geoscience, University of Calgary
[2]Dept. of Physics and Astronomy, University of Calgary

Summary

Event size is a fundamental parameter in seismic analysis. Various measures of event size exist, however the most basic parameter is the scalar seismic potency. A relationship between potency and moment magnitude (obtained via moment tensor inversion) is derived for a microseismic dataset acquired during hydraulic fracturing. The results are compared with an earthquake catalog from southern California. Preliminary results suggest that the two datasets do not scale linearly over a broad magnitude range. This may be due to small magnitude events being more susceptible to small variations in the stress field.

Introduction

Determining the size or magnitude of a seismic event is one of the most fundamental tasks in seismic analysis, as it not only provides an estimation of fracture size but can also be important for seismic hazard mitigation. Event size can be quantified in numerous ways, however the most commonly used parameter is the scalar seismic moment, M_0, which is defined as:

$$M_0 = \mu \bar{S} A, \tag{1}$$

where μ is the effective rigidity of the source volume, $\bar{S}$ is the average slip on the fault, and A is the rupture area (Aki and Richards, 2002). A more basic measure of event size is defined by the scalar seismic potency, P_0, which is simply the product of the average slip on the fault and the rupture area (Ben-Menahem and Singh, 1981), so that:

$$P_0 = \bar{S} A = M_0/\mu \, . \tag{2}$$

Unlike the scalar seismic moment, potency is a directly observable quantity as it does not require any assumptions to be made on the material properties (i.e. the effective rigidity) of the source (Ben-Zion, 2001). Both the scalar seismic potency and the seismic moment are proportional to the low-frequency amplitude plateau of the far-field displacement spectrum (Aki and Richards, 2002), and are useful for further determining important source attributes such as stress/strain drop, the radius of the fault rupture, and radiated seismic energy.

Kanamori (1977) introduced the concept of moment magnitude, M_w, which was the first magnitude parameter to be derived from a physical source characteristic rather than from empirical measurements (such as local magnitude M_L),. Hanks and Kanamori (1979) defined a relationship between the scalar seismic moment (in units of Nm) and moment magnitude:

$$M_w = \frac{2}{3} \log M_0 - 6.7 \, , \tag{3}$$

so that the obtained moment magnitude values are approximately equivalent to M_L values of moderate to large earthquakes. This relationship led to the moment magnitude scale that is widely used throughout seismology today; however, it is important to note that equation 3 does not properly characterize the

relationship between moments and local magnitudes of small events ($< M_L$ 3.5) (Hanks and Boore, 1984; Ben-Zion and Zhu, 2002; Ross et al., 2016, and references therein).

As shown in equations 1 to 3, in order to calculate the scalar seismic moment and in turn the moment magnitude of an event, one must first calculate the seismic potency and then multiply the obtained result by an assumed rigidity. However, different analysts can assume different rigidity values for the same earthquake, which can result in varying estimates of seismic moment and moment magnitude. This results in an artificial scatter propagating into recorded moment values, thus making it difficult to compare moment magnitude values from different studies (Ben-Zion, 2001). It is therefore important to derive relationships between magnitudes and potency, rather than moment, to obtain a faithful physical representation of the size of the source.

Ben-Zion and Zhu (2002) found that magnitudes only scale linearly with potency over two to three orders of magnitude for earthquakes in southern California, and that a quadratic scaling relationship may be more appropriate over broader magnitude ranges. This could potentially be due to increasingly larger events being associated with increasingly smoother stress fields, and that small-scale fluctuations in the stress field are more likely to limit the growth of slip with rupture area for smaller events, rather than for larger events (Fisher et al., 1997). In other words, potency could only be proportional to the rupture area for small events, whereas for larger events potency is proportional to the product of the rupture area and slip (Ben-Zion and Zhu, 2002).

Potency-magnitude studies have only been carried out in the $0 < M_L < 6$ range (Ben-Zion and Zhu, 2002); Ross et al., 2016), therefore in this study we aim to develop a relation between potency and magnitude for events in the microseismic range using a hydraulic fracturing microseismic dataset from the Barnett Shale, Fort Worth Basin, Texas.

Data

Microseismic data acquired during multistage hydraulic fracturing of two horizontal wells in the Barnett Shale, Fort Worth Basin, Texas is presented. The hydraulic fracturing treatment was monitored by two vertical downhole arrays, with 40 three-component 15 Hz geophones in each vertical array. Over 7000 microseismic events (MSEs) were detected by the monitoring array and were subsequently processed and analyzed by the microseismic vendor. Moment tensor inversion (MTI) was also performed on the MSEs and the corresponding solutions, together with a moment magnitude value derived from a waveform fit, were included in the MSE catalog. In this study, all of the catalogued events are extracted from the continuous data recordings, and over 1400 of the largest events (magnitudes in the range -1.7 < M_w < -0.5) are picked for P- and S-phase arrival times from the three-component seismic data.

Method

An idealized far-field body wave spectra from a seismic dislocation on a small penny-shaped crack, has three distinguishing features: a low-frequency amplitude plateau, Ω_0, a corner frequency, f_c, and a high frequency spectral fall-off, n (Figure 1). These parameters can be described by the Brune source model (Brune, 1970) as:

$$A_f = \frac{\Omega_0 \, e^{-\pi f t/Q}}{1+ (f/f_c)^n} \quad , \tag{4}$$

where A_f is the displacement amplitude spectrum, t is the travel-time from the source to the receiver, Q is the seismic quality factor, and f is the frequency. The Brune source model assumes a value of n = 2, however estimating the spectral falloff and corner frequency parameters are outside the scope of this study and will not be addressed from hereon. The seismic potency is proportional to Ω_0 (Aki and Richards, 2002) as:

$$P_0 = \frac{4\pi v r \Omega_0}{R} \quad , \tag{5}$$

where v is the P- or S-wave velocity, r is the source-to-receiver distance, and R is the a coefficient correcting the observed amplitudes for the influence of the P- or S-wave radiation pattern of the seismic source (Hanks and Kanamori, 1979).

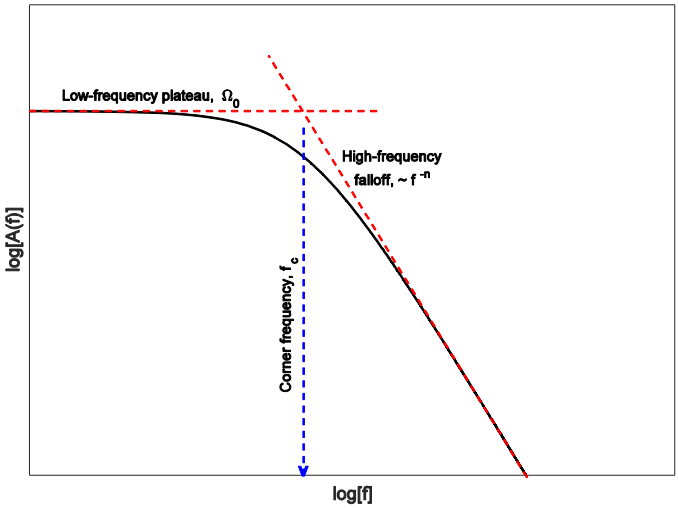

Figure 1: *Relationship of Brune source model parameters to an idealized far-field displacement spectra for shear or tensile dislocation on a penny-shaped crack.*

Displacement spectra are hence calculated for the P- and S-phases of each individual event and sensor using a multitaper method. The displacement amplitude spectra for the three components of each sensor are combined using:

$$D = \sqrt{H_1^2 + H_2^2 + Z^2}\,, \tag{6}$$

where D is the combined displacement amplitude spectrum for the sensor and H_1 and H_2 are the horizontal components and Z is the vertical component. This results in a set of P- and S-wave amplitude displacement spectra for each event. For each displacement spectra, Ω_0 is estimated by taking the median value of D in the 20-30 Hz frequency band. This frequency range is chosen to ensure that the measured amplitudes are above the 15 Hz limit of the geophones, and below the corner frequency of the largest event. Potency is determined from Ω_0 for each phase on each sensor using equation 5, assuming a P-wave velocity of 5000 ms^{-1}, a S-wave velocity of $v_p/\sqrt{3}$, R_p and R_s of 0.52 and 0.63, respectively (which are the spherically averaged point-source radiation pattern values for a shear crack (Boore and Boatwright, 1984)). Median potency values are subsequently calculated for each phase and averaged to obtain the final potency value for that event.

Results

Potency-magnitude relationships have predominantly been derived for potency versus local magnitude. M_L is derived from a measure of peak amplitude of a seismogram and corrected for source-receiver distance, however it is not directly related to a physical source property. As local magnitude values are not standardly calculated for MSEs, in this study we choose to plot our potency values against the moment magnitude values that were obtained via MTI. The moment tensor solution is determined via waveform fitting and is representative of the source process; hence moment magnitude obtained via MTI should be a superior substitute for M_L. The relationship between the log of potency and magnitude for 1414 MSEs is shown in Figure 2. The obtained potency values appear more scattered with decreasing magnitude, which may be due to noise propagating into the data. Nevertheless, a linear trend between potency and magnitude can be observed, with a line of best fit (obtained via linear regression) having a gradient of 0.78.

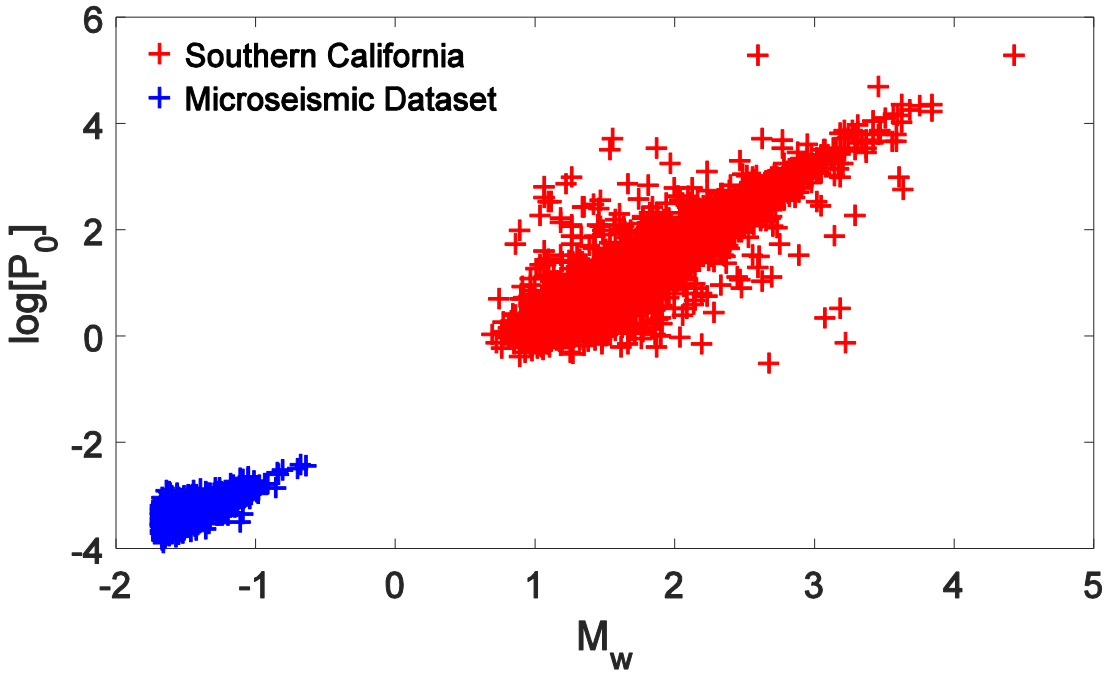

Figure 2: *Potency-moment magnitude plot for > 1400 microseismic events acquired during hydraulic fracturing (blue crosses) and > 11,000 earthqaukes from southern California (red crosses).*

Discussion and Conclusion

The MSEs recorded in hydraulic fracturing environments, only span a relatively small magnitude range in comparison to regional seismic catalogs. A potentially linear relationship between potency and magnitude can be observed over the small magnitude range available, however the data appears noisier with decreasing magnitude. A non-linear relationship could potentially be observed over a broader magnitude range. In order to investigate potency-magnitude relationships over a wider magnitude range, the microseismic data is plotted together with potency-magnitude data obtained for > 11,000 earthquakes recorded in southern California by Ross et al. (2016) (Figure 2). As mentioned earlier, most studies relate potency with local magnitude, therefore the M_L values are converted to M_w using the scaling relationship derived by Ross et al. (2016).

To the first order, the potency-magnitude values for the two datasets appear to correlate well. A line of best fit with a gradient of 1.4, obtained via linear regression, can be derived. However, as the southern California event catalog contains approximately eleven times more events than the MSE catalog, the linear regression is likely to be more biased towards fitting the southern California catalog data. In order to test this theory, linear regression analysis is performed on the “corrected” southern California earthquake data alone, resulting in a line of best fit with a gradient of 1.5, which is very similar to that obtained for the combined catalog. This value is almost twice of that determined for the microseismic data alone suggesting that seismic event size in the microseismic range does not scale linearly with regional seismicity.. The much lower gradient obtained for the MSEs is expected when the failure process is more disordered due to a fluctuating stress field (Fisher et al., 1997).

Acknowledgements

The authors would like to thank the sponsors of the Microseismic Industry Consortium for financial support. We are grateful to ConocoPhillips for providing the microseismic dataset used in this study.

References

Aki, K., and Richards, P. G., 2002, Quantitative Seismology: University Science Books, second edition.

Ben-Menahem, A., and Singh, S. J., 1981, Seismic waves and sources: Springer Verlag, New York.

Ben-Zion, Y., and Zhu, L., 2002, Potency-magnitude scaling relations for southern California earthquakes with 1.0 < M L < 7.0: Geophys. J. Int, 148, 1–5.

Ben-Zion, Y., 2001, A note on quantification of the earthquake source: Seismological Research Letters, 72, no. 2, 151–152.

Boore, D. M., and Boatwright, J., 1984, Average bodywave radiation coefficients: Bulletin of the Seismological Society of America, 74, no. 5, 1615–1621.

Brune, J. N., 1970, Tectonic stress and the spectra of seismic shear waves from earthquakes: Journal of Geophysical Research, 75, no. 26, 4997–5009.

Fisher, D., Dahmen, K., Ramanathan, S., and Ben-Zion, Y., 1997, Statistics of Earthquakes in Simple Models of Heterogeneous Faults: Physical Review Letters, 78, no. 25, 4885–4888.

Hanks, T. C., and Boore, D. M., 1984, Moment-magnitude relations in theory and practice: Journal of Geophysical Research, 89, no. B7, 6229.

Hanks, T. C., and Kanamori, H., 1979, A moment magnitude scale: Journal of Geophysical Research: Solid Earth, 84, no. B5, 2348–2350.

Kanamori, H., jul 1977, The energy release in great earthquakes: Journal of Geophysical Research, 82, no. 20, 2981–2987.

Ross, Z. E., Ben-Zion, Y., White, M. C., and Vernon, F. L., 2016, Analysis of earthquake body wave spectra for potency and magnitude values : Implications for magnitude scaling relations: Geophysical Journal International, pages 1–16.